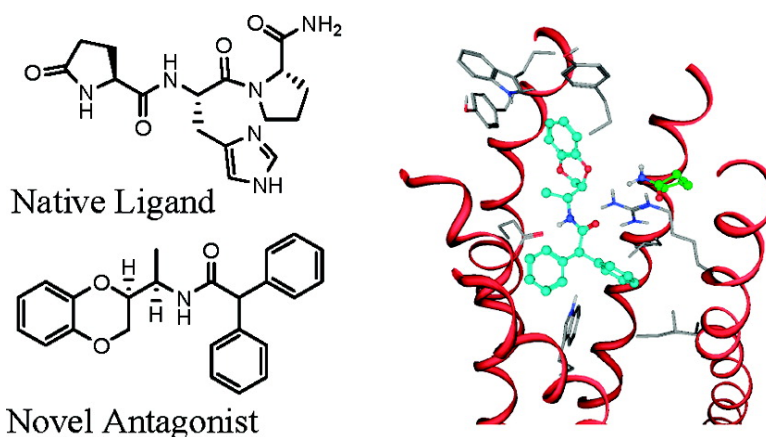


A Virtual Screen for Diverse Ligands: Discovery of Selective G Protein-Coupled Receptor Antagonists

Stanislav Engel, Amanda P. Skoumbourdis, John Childress, Susanne Neumann, Jeffrey R. Deschamps, Craig J. Thomas, Anny-Odile Colson, Stefano Costanzi, and Marvin C. Gershengorn

J. Am. Chem. Soc., **2008**, 130 (15), 5115-5123 • DOI: 10.1021/ja077620l • Publication Date (Web): 22 March 2008

Downloaded from <http://pubs.acs.org> on February 8, 2009



More About This Article

Additional resources and features associated with this article are available within the HTML version:

- Supporting Information
- Access to high resolution figures
- Links to articles and content related to this article
- Copyright permission to reproduce figures and/or text from this article

[View the Full Text HTML](#)

A Virtual Screen for Diverse Ligands: Discovery of Selective G Protein-Coupled Receptor Antagonists

Stanislav Engel,[†] Amanda P. Skoumbourdis,[‡] John Childress,[†] Susanne Neumann,[†] Jeffrey R. Deschamps,[§] Craig J. Thomas,[‡] Anny-Odile Colson,[†] Stefano Costanzi,[†] and Marvin C. Gershengorn^{*†}

The Clinical Endocrinology Branch and Laboratory of Biological Modeling, National Institute of Diabetes and Digestive and Kidney Diseases, National Institutes of Health, 50 South Drive, Bethesda, Maryland 20892, NIH Chemical Genomics Center, National Human Genome Research Institute, National Institutes of Health, 9800 Medical Center Drive, Rockville, Maryland 20850, and Laboratory for the Structure of Matter, Naval Research Laboratory, Washington, D.C. 20375

Received October 3, 2007; E-mail: marving@intra.niddk.nih.gov

Abstract: Virtual screening has become a major focus of bioactive small molecule lead identification, and reports of agonists and antagonists discovered via virtual methods are becoming more frequent. G protein-coupled receptors (GPCRs) are the one class of protein targets for which success with this approach has been limited. This is likely due to the paucity of detailed experimental information describing GPCR structure and the intrinsic function-associated structural flexibility of GPCRs which present major challenges in the application of receptor-based virtual screening. Here we describe an in silico methodology that diminishes the effects of structural uncertainty, allowing for more inclusive representation of a potential docking interaction with exogenous ligands. Using this approach, we screened one million compounds from a virtual database, and a diverse subgroup of 100 compounds was selected, leading to experimental identification of five structurally diverse antagonists of the thyrotropin-releasing hormone receptors (TRH-R1 and TRH-R2). The chirality of the most potent chemotype was demonstrated to be important in its binding affinity to TRH receptors; the most potent stereoisomer was noted to have a 13-fold selectivity for TRH-R1 over TRH-R2. A comprehensive mutational analysis of key amino acid residues that form the putative binding pocket of TRH receptors further verified the binding modality of these small molecule antagonists. The described virtual screening approach may prove applicable in the search for novel small molecule agonists and antagonists of other GPCRs.

Introduction

A recent survey of known drug targets confirmed G protein-coupled receptors (GPCRs or seven transmembrane-spanning receptors) as the most widely targeted class of cellular proteins by pharmacological agents.¹ The cell surface accessibility of the GPCR extracellular domain and seven transmembrane helices, as well as the control of wide-ranging physiological processes that are engendered by GPCR activation or inhibition, provides strong rationale for the “drugability” of this cellular target. While the completion of the human genome and other milestones in cellular and molecular biology has advanced our understanding of cellular targets, so too have advances in the drug discovery process. Traditional efforts rooted in the screening of small molecules against specific cellular targets have been joined by novel technologies, including structure-based methods² and virtual or in silico screening approaches.³ High-throughput screening is, perhaps, the most powerful method for identifying small molecule ligands that possess intrinsic biochemical

activity.⁴ However, screening efforts on a large scale are often prohibitively expensive and technically inaccessible to all but the industrial sector and singular screening efforts within the NIH Molecular Libraries Initiative.⁵ Structure or fragment-based drug design is more accessible; however, targets such as GPCRs, for which crystallographic or NMR-based structural information is difficult to generate, are not readily studied by such methods. Thus, it is difficult to discover small molecule ligands for these compelling pharmacological targets.

The recent success of in silico methods in identifying compound leads for targets such as kinases⁶ and transcription factors⁷ has highlighted the mainstream use of virtual screening.

(2) Congreve, M.; Murray, C. W.; Blundell, T. L. *Drug Discovery Today* **2005**, *10*, 895–907.

(3) Muegge, I.; Oloff, S. *Drug Discovery Today: Technol.* **2006**, *3*, 405–411.

(4) Inglesse, J.; Johnson, R. L.; Simeonov, A.; Xia, M.; Zheng, W.; Austin, C. P.; Auld, D. S. *Nat. Chem. Biol.* **2007**, *3*, 466–479.

(5) Austin, C. P.; Brady, L. S.; Insel, T. R.; Collins, F. S. *Science* **2004**, *306*, 1138.

(6) Toledo-Sherman, L.; Derety, E.; Slon-Usakiewicz, J. J.; Ng, W.; Dai, J.-R.; Foster, J. E.; Redden, P. R.; Uger, M. D.; Liao, L. C.; Pasternak, A.; Reid, N. *J. Med. Chem.* **2005**, *48*, 3221–3230.

(7) Derksen, S.; Rau, O.; Schneider, P.; Schubert-Zsilavecz, M.; Schneider, G. *ChemMedChem* **2006**, *1*, 1346–1350.

[†] National Institute of Diabetes and Digestive and Kidney Diseases.

[‡] National Human Genome Research Institute.

[§] Naval Research Laboratory.

(1) Imming, P.; Sinning, C.; Meyer, A. *Nat. Rev. Drug Discovery* **2007**, *5*, 821–834.

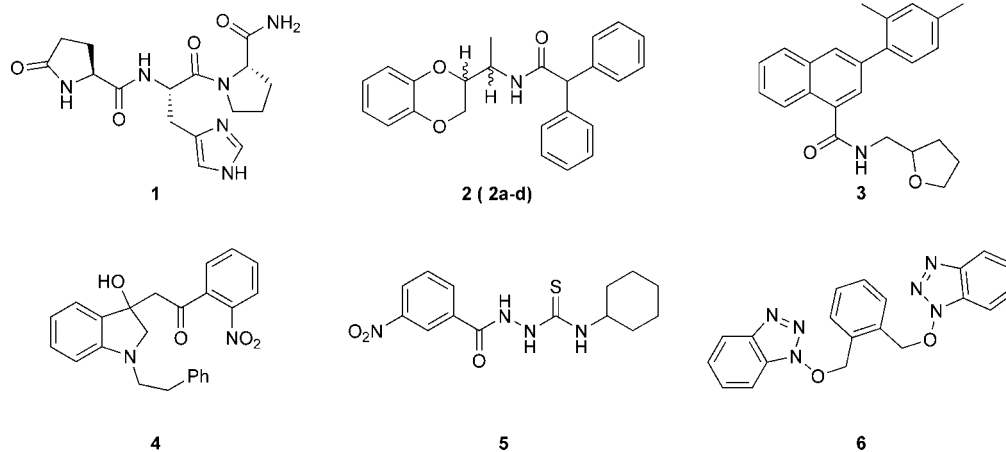


Figure 1. Compound structures of thyrotropin-releasing hormone (**1**) and the compounds identified by the virtual screen.

Proteins with well-documented crystallographic or NMR-based structures constitute the most successfully pursued targets of virtual screening. In the absence of protein structural information, an alternate virtual screening format utilizes detailed knowledge of known ligands and is commonly referred to as ligand-based virtual screening.³ There is little ability to establish a virtual screen in cases where protein structure is unavailable and ligand classes have yet to be discovered. Few reports of in silico generated ligands of GPCRs have been reported,^{8–11} most likely due to the paucity of information of the structure of the receptors. For several years, the only experimentally delineated GPCR structure was that of rhodopsin¹² (a class A GPCR). Recently, after this work was completed, crystal structures for the human β_2 -adrenergic receptor (β_2 -AR) have also been published.^{45–47} These findings disclosed a substantial structural similarity between rhodopsin and the β_2 -AR, amply supporting the widespread practice of modeling GPCRs by homology.

Although homology modeling has gained sophistication and credibility in recent years and new techniques for GPCR structural modeling continue to evolve,¹³ these advances have yet to generate widespread success in GPCR virtual screens. At least three factors contribute to the limited applicability of in silico GPCR methods. The first factor is the inherent conformational flexibility of GPCRs. The idea of induced fit for both receptor and ligand may represent a general feature of GPCR activation, and the ligand binding pocket of a GPCR may have intrinsic plasticity, resulting in the ability to adopt a number of alternative conformations. Consequently, there is a high level of uncertainty surrounding an exact designation of a receptor-based pharmacophore. Moreover, the use of static representations of receptor/ligand complexes as templates for formulation of a pharmacophore hypothesis may erroneously restrict the available binding potential. Shoichet and co-workers have introduced technical advances in “soft docking” to aid

virtual methods in overcoming these issues.¹⁴ The second factor involves the availability of multiple sites of binding interaction within the transmembrane binding cavity of GPCRs. An approach that includes the entire binding potential of the putative binding pocket may allow for the discovery of ligands that bind to the receptor via interactions not exploited by the cognate ligand. The third factor, which does not concern GPCRs exclusively, is the inherent inaccuracy of the scoring functions. While a number of docking procedures proved capable of reproducing the geometry of receptor–ligand complexes, the associated scoring functions are not yet a viable solution for predicting affinity of the ligands.^{48,49} This is especially true when the structures of the receptors are derived by homology modeling.

Thyrotropin-releasing hormone (TRH), Figure 1, plays an important role in the regulation of thyrotropin (thyroid-stimulating hormone, TSH) and prolactin synthesis and secretion in the pituitary gland and as a neurotransmitter/neuromodulator within the central and peripheral nervous systems.¹⁵ TRH action is mediated by the two TRH receptor isotypes, TRH-R1 and TRH-R2. On the basis of the marked differences in tissue distribution and basal signaling of TRH-R1 and TRH-R2, it is likely that the two receptors mediate differing effects of TRH.¹⁶ A potent, efficacious small molecule ligand with selectivity between TRH-R1 and TRH-R2 would be of use to delineate the unique physiological roles of each receptor. In addition, nonpeptide TRH receptor ligands, which are metabolically stable and able to cross the blood–brain barrier, might be valuable for the treatment of several neuropathological conditions including neurodegeneration. Thus, novel TRH receptor agonists and/or antagonists would be of general use to the biomedical community.

In this study, we applied a virtual screening approach to identify novel small molecule ligands of TRH-R1 and TRH-R2, with a particular interest in identifying isotype-selective ligands.

Structural alignment of the binding cavities of TRH-R1 and TRH-R2 has revealed that the composition and arrangement of residues within the transmembrane domains (TMDs) that are important for TRH binding are nearly identical.¹⁷ This is

(8) Marriott, D. P.; Dougall, I. G.; Meghani, P.; Liu, Y.-J.; Flower, D. R. *J. Med. Chem.* **1999**, *42*, 3210–3216.

(9) Freddolino, P. L.; Kalani, M. Y. S.; Vaidehi, N.; Floriano, W. B.; Hall, S. E.; Trabanino, R. J.; Kam, V. W. T.; Goddard, W. A. *Proc. Natl. Acad. Sci. U.S.A.* **2004**, *101*, 2736–2741.

(10) Evers, A.; Klebe, G. *J. Med. Chem.* **2004**, *47*, 5381–5392.

(11) Evers, A.; Hessler, G.; Matter, H.; Klabunde, T. *J. Med. Chem.* **2005**, *48*, 5448–5465.

(12) Palczewski, K.; Kumasaka, T.; Hori, T.; Behnke, C. A.; Motoshima, H.; Fox, B. A.; Le, T. I.; Teller, D. C.; Okada, T.; Stenkamp, R. E.; Yamamoto, M.; Miyano, M. *Science* **2000**, *289*, 739–745.

(13) Zhang, Y.; DeVries, M. E.; Skolnick, J. *PLoS Comp. Biol.* **2006**, *2*, 88–99.

(14) Ferrari, A. M.; Wei, B. Q.; Costantino, L.; Shoichet, B. K. *J. Med. Chem.* **2004**, *47*, 5076–5084.

(15) Metcalf, G.; Jackson, I. M. D. *Ann. N.Y. Acad. Sci.* **1989**, 533.

(16) Sun, Y.; Lu, X.; Gersengorn, M. C. *J. Mol. Endocrinol.* **2003**, *30*, 87.

(17) Engel, S.; Gershengorn, M. C. *Pharmacol. Ther.* **2007**, *113*, 410–419.

consistent with the observed binding affinity similarities for TRH and its numerous analogues at these two receptors.¹⁶ Thus, a virtual screen utilizing a ligand binding cavity with binding potentials distinct from those utilized by TRH may be beneficial for the discovery/design of novel, diverse and selective modulators of TRH receptor activities.

Our screening was based on a homology model of TRH-R1 previously built based upon a 3D projection map of bovine rhodopsin as structural template.¹⁸ Numerous studies exploring both chemically modified TRH and mutationally altered receptors have allowed detailed assessment and refinement of the predicted binding cavity.^{19–26}

Overall, the screening comprised four sequential stages: two actual virtual screenings, each of which was followed by a diverse subset selection (Supplementary Figure 1). Each stage was designed to reduce the input virtual library of compounds to 10% of its size. To mitigate the limits of currently used procedures, our virtual screening scheme was designed to (a) consider receptor flexibility; (b) take into account all the available binding potential of the ligand binding cavity; and (c) minimize the use of scoring functions by integrating them with selections based on pharmacophore matching and diversity.

The virtual screening led to experimental identification of five structurally diverse antagonists of TRH receptors. In particular, a stereoisomer of *N*-(1-(2,3-dihydrobenzo[*b*][1,4]dioxin-2-yl)ethyl)-2,2-diphenylacetamide was identified as a novel, potent, and selective small molecule antagonist of TRH-R1.

Methods

Modeling: Virtual Screening. A model of the TRH/TRH-R1 complex based on the topological homology to the 3D projection map of rhodopsin was used as the structural template for this study. This model was obtained through a series of optimizations using various computer simulation techniques to rationalize the effects of complementary modifications in the structure of TRH and TRH-R1.^{18,20}

Here, a receptor-based pharmacophore describing the interaction potential of the TRH-R1 binding pocket was generated using the combination of the programs Grid (Molecular Discovery)²⁷ and Unity (Sybyl 7.1).²⁸ A box of $15 \times 15 \times 15 \text{ \AA}^3$ was defined around the position of TRH in the complex. After TRH extraction, the potential to form hydrophobic, proton donor or proton acceptor interactions within the box was explored using “dry”, neutral flat NH_2 and sp^2 carbonyl oxygen molecular probes, respectively (Grid). The effective dielectric constant was set to 8.0. Flexibility of the side chains was allowed, thereby extending the area of potential interactions. A methyl (CH_3) molecular probe was used to define the van der Waals boundaries of the binding cavity. Within this

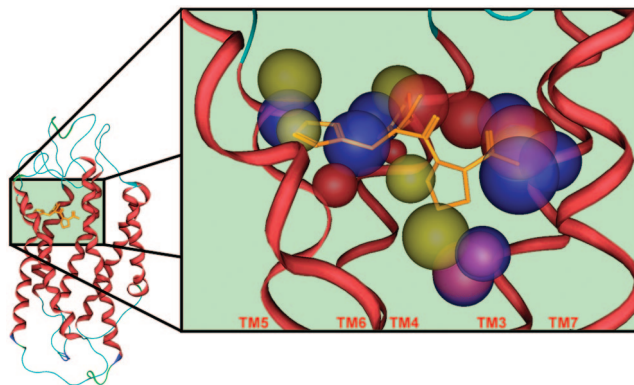


Figure 2. Interaction potential (receptor-based 3D pharmacophore) of the ligand binding cavity in TRH-R1. Blue, red, and yellow spheres represent a potential field of interaction with H-donor, H-acceptor, and hydrophobic molecular probes, respectively. TRH (in orange) is superimposed with the receptor-based pharmacophore, demonstrating that only a part of the available interaction potential is utilized for TRH binding. Flexibility was granted to the residues lining the binding pocket in the calculation of the interaction potentials.

cavity, the clustering points of high potential interaction energy for each molecular probe (less than -0.1 kcal/mol for the “dry” probe, less than -7 kcal/mol for the NH_2 probe, and less than -12 kcal/mol for the carbonyl oxygen probe) were represented as spherical features of corresponding radius using Unity and combined into a single query (Figure 2). This spherical representation of the interaction potential mimics the entire conformational space of the key residues, thus addressing the issue of protein flexibility in the ligand docking and partially compensating for model imprecision. The partial-match constraints protocol (Unity) was used to define four distinct groups, reflecting the spatial localization of the spherical features.

One million commercially available compounds from the ZINC database of diverse drug-like compounds²⁹ were screened using the Flex Search protocol (Unity) with the conformational space of the ligands sampled in an attempt to fulfill all the partial-match constraints. The partial constraints in the query were empirically set to produce a hit rate of 10% ($\sim 100\,000$ compounds). Only ligands concurrently matching from 1 to 3 spherical features in each partial query were considered as “hits”. A 10% diverse subset ($\sim 10\,000$ compounds) of the Unity pharmacophoric search hit-list was subsequently evaluated by flexible docking to the putative TRH binding pocket in TRH-R1 using the program FlexE (Tripos).³⁰ The selection of this subset was carried out based on the position of the compounds in 6D chemical space, defined by the six optimized BCUT descriptors (elecneg_S_burden_001.000_K_H; elecneg_S_invtpd_000.100_K_L; gastchrg_S_invtpd_000.010_K_H; gastchrg_S_invtpd_010.000_K_L; tabpolar_S_burden_001.000_K_L; tabpolar_S_invdist_000.250_K_H) using a methodology implemented in the Diverse Solution software³¹ available within Sybyl 7.1.³² During docking with FlexE, flexibility of the ligands was allowed and the binding pocket was represented by an assembly of the five alternative conformations in order to mimic flexibility of the protein target (see Generation of Alternative Conformations of the Binding Cavity). The FlexX scoring function was used to evaluate the compound–receptor interaction in the docking procedure. One thousand compounds with docking scores higher than 26 kJ/mol were selected (the interacting energy for TRH was 28 kJ/mol), and a 10% diverse subset (100 compounds) was generated using MACCS structural keys fingerprints (Tanimoto coefficient

(18) Colson, A. O.; Perlman, J. H.; Smolyar, A.; Gershengorn, M. C.; Osman, R. *Biophys. J.* **1998**, *74*, 1087–1100.

(19) Rutledge, L. D.; Perlman, J. H.; Gershengorn, M. C.; Marshall, G. R.; Moeller, K. D. *J. Med. Chem.* **1996**, *39*, 1571–1575.

(20) Perlman, J. H.; Laakkonen, L. J.; Guarnieri, F.; Osman, R.; Gershengorn, M. C. *Biochemistry* **1996**, *35*, 7643–7650.

(21) Laakkonen, L. J.; Guarnieri, F.; Perlman, J. H.; Gershengorn, M. C.; Osman, R. *Biochemistry* **1996**, *35*, 7651–7663.

(22) Perlman, J. H.; Colson, A.-O.; Wang, W.; Bence, K.; Osman, R.; Gershengorn, M. C. *J. Biol. Chem.* **1997**, *272*, 11937–11942.

(23) Colson, A.-O.; Perlman, J. H.; Jinsi-Parimoo, A.; Nussenzveig, D. R.; Osman, R.; Gershengorn, M. C. *Mol. Pharmacol.* **1998**, *54*, 968–978.

(24) Jain, R.; Singh, J.; Perlman, J. H.; Gershengorn, M. C. *Bioorg. Med. Chem.* **2002**, *10*, 189–194.

(25) Kaur, N.; Lu, X.; Gershengorn, M. C.; Jain, R. *J. Med. Chem.* **2005**, *48*, 6162–6165.

(26) Kaur, N.; Monga, V.; Lu, X.; Gershengorn, M. C.; Jain, R. *Bioorg. Med. Chem.* **2007**, *15*, 433–443.

(27) *Grid 1.2.2*; Molecular Discovery Ltd.: Oxford, U.K., 1998.

(28) *Unity*; Tripos Inc.: St. Louis, MO 63144, 2006.

(29) Irwin, J. J.; Shoichet, B. K. *J. Chem. Inf. Model.* **2005**, *45*, 177–182.

(30) *FlexE*; Tripos Inc.: St. Louis, MO 63144, 2006.

(31) Pearlman, R. S.; Smith, K. M. *Perspect. Drug Discovery Des.* **1998**, *9*, 339–353.

(32) *Sybyl 7.1*; Tripos Inc.: St. Louis, MO 63144, 2006.

similarity metric) implemented in the Diverse Subset feature of MOE³³ and submitted to experimental testing.

Generation of Alternative Conformations of the Binding Cavity. A conformational search of the residues lining the receptor cavity as defined by a methyl (CH₃) molecular probe (Grid) was conducted with the Monte Carlo Multiple Minima (MCOMM) protocol (MacroModel 9.1, Schrödinger).³⁴ The search consisted of 1000 steps of the Monte Carlo torsional sampling intervened by 500 iterations of PRCG minimization (0.05 kJ/mol) using OPLS2005 force field in vacuum. All of the structures with an energy content higher than that of the most stable structure by more than 100 kJ/mol were rejected, as they could potentially represent geometrically distorted conformations. Of the remaining structures, the most stable one and the four most diverse, in terms of atomic rmsd, were selected for docking studies. The five selected structures showed rmsd values of about 0.4 Å from each other. This is indicative of significant diversity, considering that only the residues lining the binding pocket were involved in the conformational search (the rest of the protein was frozen), and the rmsd values were calculated with respect to all the atoms of the receptor. The selection of five diverse structures was judged sufficient since the FlexE docking program combines them to generate a higher number of possible alternative structures.

Neighbor Search. A search of the original library for related structures was performed using MACCS structural keys fingerprints and Tanimoto coefficient similarity metric implemented in the similarity feature of MOE.³³

Scoring of the Individual Stereoisomers of Compound 2. The LiaisonScore method (Liaison 4.0, Schrödinger)³⁵ was used to predict free binding energy of the individual stereoisomers of **2** (**2a–d**) within the model of TRH-R1. This method uses the same conformational sampling approach as the Linear Response Method (LRM)^{36,37} but is based on an empirical binding score (GlideScore)³⁸ with a discrete representation of the protein. The main advantage of the LiaisonScore over the typical docking scoring function is that it treats both ligand and protein as flexible entities, leading to a greater precision in the evaluation of protein–ligand interactions. Molecular dynamics was used as a sampling method with a temperature of 300 K. The truncated Newton algorithm was used for energy minimization. The calculations were performed with the OPLS2005 force field in a surface-generalized Born (SGB) continuum model for solvation.³⁹ Due to the absence of a set of known active compounds (training set), the calculated free binding energies have relative but not absolute meaning.

Experimental Section

Materials. Dulbecco's modified Eagle's Medium (DMEM) and fetal bovine serum were purchased from Biosource (Rockville, MD). TRH (pyroGlu-His-ProNH₂), linoleic acid (sodium salt), and luciferin were purchased from Sigma (St. Louis, MO). [³H]MeTRH was purchased from NEN Life Science Products (Boston, MA). Compounds for screening were obtained from ChemBridge (San Diego, CA) and Asinex (Winston-Salem, NC).

Construction of Vectors and Site-Directed Mutagenesis of TRH Receptor. cDNAs for mouse TRH-R1 and TRH-R2 were inserted into the pcDNA3.1(-)/hygromycin vector using restriction

sites *NcoI* and *HindIII*. Mutations were introduced using the QuikChange II XL site-directed mutagenesis kit (Stratagene). All constructs were verified by sequencing (MWG Biotech).

Cell Culture. HEK293 (human embryonic kidney) cells were grown in DMEM containing 10% fetal bovine serum, 100 units/mL penicillin, and 10 µg/mL streptomycin (Life Technologies Inc.) at 37 °C in a humidified 5% CO₂ incubator.

Ligand Binding Assays. The cells were transfected with 0.8 µg/mL of plasmid DNA encoding for TRH-R1, TRH-R2, or mutant receptors for 48 h using FuGENE6 reagent (Roche, Basel, Switzerland). Competition binding assays were performed in a monolayer of intact cells at 4 °C for 4 h with 1–5 nM [³H]MeTRH and various concentrations of test compounds as described.⁴⁰ The cells were preincubated with compound for 15 min before addition of radioligand. Equilibrium dissociation constants (*K_d*) for [³H]MeTRH were determined in saturation binding experiments as described⁴¹ or in competition experiments using unlabeled MeTRH. Equilibrium binding constants for tested compounds were derived using the formula: $K_i = (IC_{50}) / (1 + ([L]/K_d))$, where *IC*₅₀ is the concentration of unlabeled ligand that half-competes with specifically bound [³H]MeTRH, and *K_d* is the equilibrium dissociation constant for [³H]MeTRH.

Luciferase Assay. HEK293 cells were transfected with 0.8 µg/mL of plasmid DNA encoding for TRH-R1 or TRH-R2 and 0.8 µg/mL of pAP(Activator Protein)-1Luc vector (PathDetect In Vivo Signal Transduction Pathway *trans*- and *cis*-Reporting System; Stratagene, La Jolla, CA). After 6 h of transfection, the cells were stimulated with or without 3 nM TRH in the presence or absence of 30 µM of **2** and incubated for an additional 18 h. The luminescence was measured as previously described.⁴²

Measurement of Intracellular Calcium Mobilization Using Fluorometric Imaging Plate Reader (FLIPR^{TETRA}). HEK293 cells stably expressing TRH-R1, TRH-R2, or GPR40 were seeded in black-walled, clear-bottomed 96-well plates (Corning, NY) at a density of 6 × 10⁴ cells/well in DMEM with 10% fetal bovine serum and incubated for 24 h at 37 °C and 6% CO₂. The following day, the culture media was replaced with 100 µL of Hank's Balanced Salt Solution with 20 mM HEPES, and the cells were loaded with 100 µL of calcium 3 fluorescent dye (Molecular Devices, Sunnyvale, CA) for 1 h at room temperature before addition of compounds. Transient changes in [Ca²⁺] induced by ligands were measured using the FLIPR^{TETRA} system (Molecular Devices, Sunnyvale, CA). Changes in fluorescence were detected at the emission wavelength of 515–575 nm. Agonistic and antagonistic properties of ligands were measured in a concentration range from 10 nM to 50 µM. The agonistic response was determined immediately upon compound addition, followed by 15 min continued incubation before addition of EC₅₀ concentration of TRH (1 nM, TRH receptors) or linoleic acid (10 µM, GPR40) to measure antagonistic effects. Responses were measured as peak fluorescent intensity minus basal fluorescent intensity at each compound concentration.

Data Analysis. All data were analyzed by linear or nonlinear regression using the Prism software version 3 (GraphPad, Inc., San Diego, CA).

Results and Discussion

To achieve a robust and reliable virtual screen for ligands of a GPCR, there must exist a detailed model of the core putative binding pocket. From our longstanding efforts to dissect the binding of TRH (**1**) (Figure 1) to TRH-R1,^{18–26} an experimentally supported homology model was available and was used in the virtual screen. As discussed, a four-stage virtual screening

(33) *Molecular Operating Environment*; Chemical Computing Group, Inc.: Montreal Quebec, Canada, 2005.

(34) *MacroModel 9.1*; Schrödinger, LLC.: New York, 2003.

(35) *Liaison 4.0*; Schrödinger, LLC.: New York, 2005.

(36) Aqvist, J.; Medina, C.; Samuelsson, J. E. *Protein Eng.* **1994**, *7*, 385–391.

(37) Jones-Hertzog, D. K.; Jorgensen, W. L. *J. Med. Chem.* **1997**, *40*, 1539–1549.

(38) Friesner, R. A.; Banks, J. L.; Murphy, R. B.; Halgren, T. A.; Klicic, J. J.; Mainz, D. T.; Repasky, M. P.; Knoll, E. H.; Shelley, M.; Perry, J. K.; Shaw, D. E.; Francis, P.; Shenkin, P. S. *J. Med. Chem.* **2004**, *47*, 1739–1749.

(39) Zhou, R.; Friesner, R. A.; Ghosh, A.; Rizzo, R. C.; Jorgensen, W. L.; Levy, R. M. *J. Phys. Chem. B* **2001**, *105*, 10388–10397.

(40) Lu, X.; Huang, W.; Worthington, S.; Drabik, P.; Osman, R.; Gershengorn, M. C. *Mol. Pharmacol.* **2004**, *66*, 1192–1200.

(41) Perlman, J. H.; Nussenzweig, D. R.; Osman, R.; Gershengorn, M. C. *J. Biol. Chem.* **1992**, *267*, 24413–24417.

(42) Gershengorn, M. C.; Osman, R. *Physiol. Rev.* **1996**, *76*, 175–191.

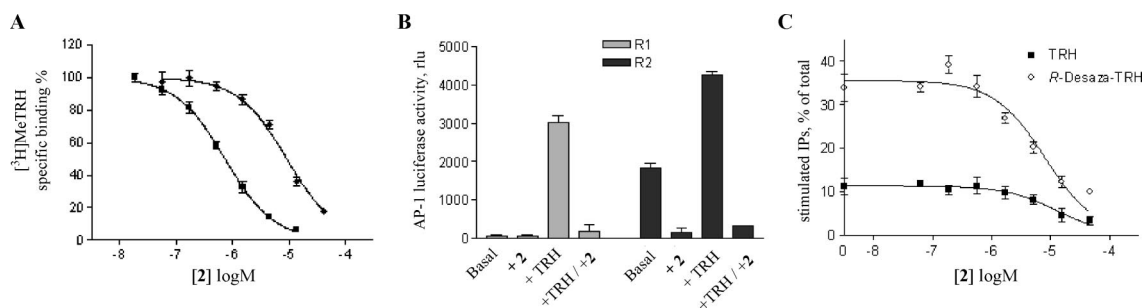


Figure 3. Pharmacological analysis of commercially available **2** that is an equal mixture **2a–d**. (A) Radioligand competition binding was performed at 4 °C in cells expressing mouse TRH-R1 (■) or TRH-R2 (◆). The cells were preincubated for 15 min with increasing concentrations of **2** followed by 4 h incubation in the presence of 1 nM [³H]MeTRH. The binding was determined as described in Methods. (B) Inhibition of TRH-stimulated signaling of TRH-R1 and TRH-R2 and of basal signaling of TRH-R2 by **2**. Luciferase activity in HEK293 cells expressing TRH-R1 or TRH-R2 was measured after stimulation with or without (basal) 3 nM TRH in the absence or presence of 30 μM of **2** as described in Methods. Rlu = relative light units. (C) Demonstration of **2** inhibiting agonist-stimulated formation of inositol phosphates. HEK293 cells expressing TRH-R1 were preincubated for 15 min with increasing concentrations of **2** followed by 90 min incubation at 37 °C in the presence of EC₅₀ concentration of TRH (2 nM) (■) or (*R*)-desaza-TRH (2.5 μM) (○). (*R*)-Desaza-TRH is a superagonist at TRH receptors (see Engel, S.; Gershengorn, M. C. *J. Biol. Chem.* **2006**, *281*, 13103). Formation of inositol phosphates was measured as described (see Engel, S.; Gershengorn, M. C. *J. Biol. Chem.* **2006**, *281*, 13103.). All of the curves represent the nonlinear regression analyses of the data using one-site competition function. All data are presented as the mean ± sem from three independent experiments performed in duplicates.

procedure (Supplementary Figure 1) was designed in order to consider the flexibility of ligands and receptor, to use the entire binding potential presented by the ligand binding cavity, and to minimize the usage of scoring functions. Molecular probes (Grid) were used to map the interaction fields associated with all amino acids lining the pocket, while granting flexibility to the side chains to account for induced fit and intrinsic uncertainty in the homology model. On the basis of this potential, a receptor-based 3D pharmacophore was generated (Figure 2). The superimposition of this pharmacophore with TRH reveals that the available interaction potential is much larger than that utilized by TRH, the cognate ligand. In the first stage of the screening, one million compounds from the ZINC database of commercially available, diverse compounds were screened virtually for flexible fitting to the receptor-based 3D pharmacophore, resulting in a hit-list of 100 000 compounds. In the second stage, a diverse subset of 10 000 compounds from this hit-list was selected to be processed in the third stage, which consisted of molecular docking at a model of the TRH-R1 binding pocket represented by an assembly of alternative conformations to mimic the structural flexibility within the binding site. To minimize the impact of scoring functions, we introduced a fourth and final stage, in which a diverse subgroup of 100 compounds among the 1000 top ranking docked compounds was selected for experimental testing.

These compounds and several related compounds (see Neighbor Search in Methods) were purchased and analyzed for their ability to stimulate TRH receptor-mediated increases in intracellular Ca²⁺, that is, act as agonists, or to inhibit TRH-stimulated increases in intracellular Ca²⁺, act as antagonists, and inhibit binding of the radiolabeled TRH analogue [³H](*N*-methyl)His-TRH using TRH-R1- and TRH-R2-expressing cells. Among the compounds tested, only antagonists were observed. We found five unique scaffolds including a novel substituted *N*-((tetrahydrofuran-2-yl)methyl)-1-naphthamide **3** and a substituted 1-phenethylindoline **4** (Figure 1) (see Supplementary Figure 2 for related IC₅₀ values). As a preliminary gauge of selectivity, we determined the level of activity of these compounds against GPR40 (a GPCR that like TRH-R1 and TRH-R2 couples to G_q⁴³) and found no activity. The assortment of chemotypes that were found to be novel antagonists of TRH-R1 and TRH-R2 strongly suggests that using an expanded binding potential and granting flexibility to the residues within

the binding cavity promotes the discovery of more diverse small molecule classes. The most compelling lead structures were based upon the core scaffold of substituted 2,3-dihydrobenzo[*b*][1,4]dioxin-2-yl (represented by compounds **2**), and several small molecules with this core structure (**11–14**, as representative compounds) were among the most highly ranked compounds from the virtual screen.

The compound **2** (*N*-(1-(2,3-dihydrobenzo[*b*][1,4]dioxin-2-yl)ethyl)-2,2-diphenylacetamide) contains two stereocenters at carbons C1 and C2 (Figure 5). The pharmacological analysis was performed utilizing a commercial preparation which included all four stereoisomers (Figure 1). This mixture was found to compete with [³H]MeTRH for binding to TRH-R1 and TRH-R2 (Figure 3A) with affinities of 0.68 ± 0.20 and 7.3 ± 1.4 μM, respectively (an 11-fold binding selectivity for TRH-R1 over TRH-R2), to inhibit TRH-mediated upregulation of expression of luciferase reporter gene and basal (ligand-independent) signaling activity of TRH-R2 (Figure 3B). The mixture of **2** was shown also to inhibit TRH and (*R*)-desaza-TRH-stimulated formation of inositol phosphate second messengers (Figure 3C). These data confirmed that the screen had indeed revealed a novel chemotype with potent and selective TRH receptor antagonism.

The presence of two chiral centers was of interest. As a preliminary study, we estimated the relative free energy of binding of each stereoisomer using molecular docking and LiaisonScore empirical scoring function. The computational analysis predicted that the C2-*S*, C1-*R* isomer **2a** would bind with the highest affinity to TRH-R1 relative to the other isomers (Figure 4A). We synthesized and tested all four individual stereoisomers of **2**. The synthesis (shown in Figure 4D) originated with chirally pure 2,3-dihydrobenzo[*b*][1,4]dioxine-2-carboxylic acids **7a** and **7b** (the *R* isomer is commercially available and the *S* isomer was obtained via a classical chiral resolution). With chiral starting materials, it was assured that one stereocenter was set. From this starting point, a Weinreb amide was formed (**8a** or **8b**) and displaced with methyl Grignard reagent to give acetates **9a** and **9b**. Reductive amination catalyzed by Ti(O^{*i*}Pr)₄ produced the primary amines **10a–d**. This step provided equal mixtures of diastereomers that

(43) Tayasam, G. V.; Tulasi, V. K.; Davis, J. A.; Bansal, V. S. *Exp. Opin. Ther. Targets* **2007**, *11*, 661–671.

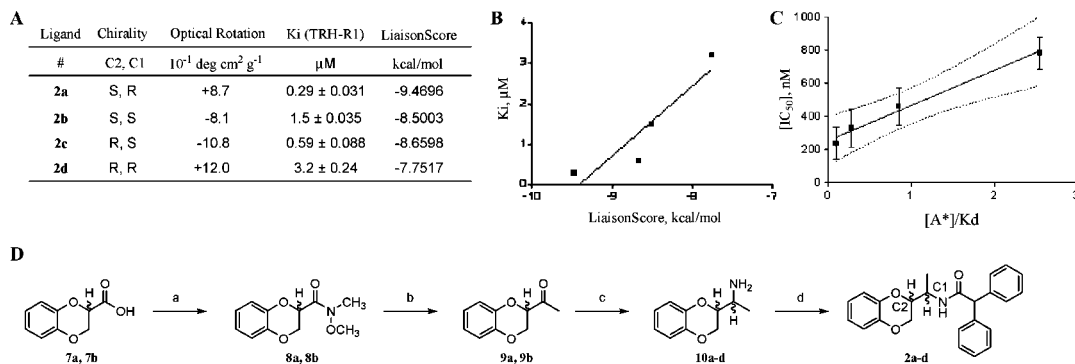


Figure 4. (A) Equilibrium binding constants and calculated LiaisonScores of **2a–d** complexes with TRH-R1. HEK293 cells were transfected for 48 h with $0.8 \mu\text{g/mL}$ of plasmid DNA encoding for TRH-R1, and equilibrium binding constants were determined as described in Methods. Data are presented as the mean \pm sem from three independent experiments performed in duplicate. LiaisonScores of the stereoisomers docked to TRH-R1 were calculated as described in Methods. (B) Linear relationship between calculated free energies of interaction (LiaisonScore) and experimental binding affinities of **2a–d**. (C) Radioligand competition binding was performed at 4°C in cells expressing mouse TRH-R1. The cells were preincubated for 15 min with increasing concentrations of **2a** followed by 4 h incubation in the presence of 0.3, 1.0, 3.0 or 10 nM [^3H]MeTRH. IC_{50} values of inhibition of radioligand binding by **2a** are directly proportional to the concentration of [^3H]MeTRH, obeying the Cheng–Prusoff relationship: $\text{IC}_{50} = K_i \times ([A^*]/K_{\text{disA}^*} + 1)$, the characteristic of competitive ligand–receptor interactions. $[A^*]$ is concentration of radioligand and K_{disA^*} is the equilibrium dissociation constant of the TRH-R1/[^3H]MeTRH complex. Data are presented as the mean \pm sem from three independent experiments performed in duplicates. Boundaries of the 95% confidence interval for the linear regression analysis are shown. (D) Synthetic scheme for the production of **2a–d**. Reagents and conditions: (a) CDI (1.1 equiv), CH_2Cl_2 , 1 h; *N,O*-dimethylhydroxylamine hydrochloride; (b) MeMgCl (1.5 equiv), THF, 0°C , 30 min; (c) $\text{Ti}(\text{O}^i\text{Pr})_4$ (2 equiv), NH_3/EtOH (5 equiv), 6 h, then NaBH_4 (1.5 equiv), 3 h; (d) diphenyl acetic acid (1.3 equiv), HATU (2 equiv), DMF, then DiPEA (3 equiv), 5 min, **6a–d** (1 equiv) in DMF dropwise, 45 min. CDI = carbonyl diimidazole; HATU = *O*-(7-azabenzotriazole-1-yl)-*N,N,N',N'*-tetramethyluronium hexafluorophosphate.

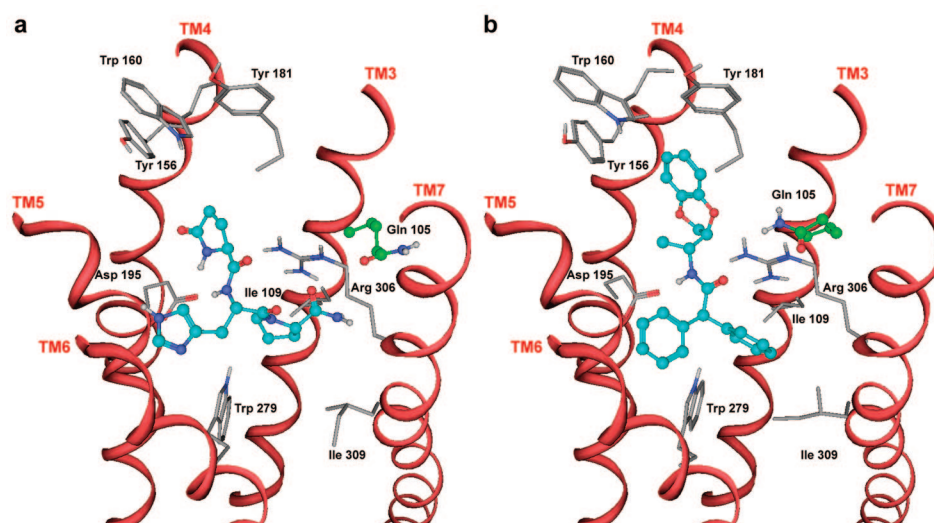
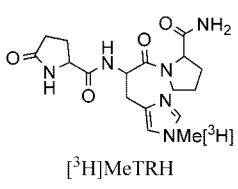
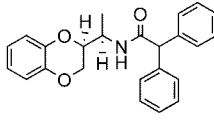


Figure 5. Models of TRH/TRH-R1 and **2a**/TRH-R1 complexes. (A) The optimized model of the TRH/TRH-R1 complex used as a starting point to design the virtual screening protocol. (B) The optimized model of the **2a**/TRH-R1 complex as generated by the virtual screening (see Methods). Note the difference in the position of Gln105 in TM-3 (in green) between the two complexes. Gln105 is not important for TRH binding but, because of its high flexibility, may contribute to binding of **2a**. In the virtual screening, the interaction field associated with Gln105 contributed to the selection of **2a** as a “hit” by superimposition with one of its dioxin oxygen atoms. In the ligands, the spheres in cyan, red, and blue correspond to carbon, oxygen, and nitrogen atoms, respectively.

were noted by LCMS analysis. Aliquots of this material were purified via LC methods, and the purified materials were crystallized. A purified, as yet undetermined crystal formed from the fast running eluent of the products derived from chirally enriched **7a** (S isomer) and crystallographic analysis revealed the structure as primarily the R,R isomer **10d** (the stereochemical designation of the C2 position changes from S to R upon reductive amination). From this structure, chiral HPLC analysis and optical rotation measurements were able to define the remaining stereoisomers. Coupling of **10a–d** with diphenyl acetic acid provided the final products **2a–d** as diastereomeric mixtures separable by LC methods. Aliquots of the purified, stereochemically defined **10a–d** were also submitted to this final procedure to allow precise definition of each final product.

The pharmacological analysis of the individual stereoisomers supported the accuracy of the model since ranking of the predicted free energies of binding was consistent with the relative affinities demonstrated by **2a–d** (Figure 4A,B). Isomer **2a** (the lead compound identified in the virtual screen) was found to have a K_i of $0.29 \mu\text{M}$ and a nearly 13-fold selectivity for TRH-R1 over TRH-R2. Compound **2a** represents the most potent inhibitor of TRH-R1 reported to date. The models of TRH-R1 complexed with TRH (**1**) or **2a** indicate overlap between the binding sites of the two ligands (Figure 5A,B). To evaluate this prediction, we determined the nature of **2a** antagonism. A linear relationship was observed between IC_{50} values for inhibition of [^3H]MeTRH binding by **2a** and

Table 1. Equilibrium Binding Constants of [³H]MeTRH and **2a** to TRH-R1, TRH-R2, and Mutant Receptors^a

	TRH-R1 mutant	TRH-R2 mutant	K _d (nM) {[³ H]MeTRH}	K _i (μM) { 2a }
 [³ H]MeTRH	WT	NA	2.0 ± 0.089	0.29 ± 0.031
	I309L	NA	6.2 ± 0.71	4.5 ± 0.29
	I309V	NA	3.9 ± 0.53	0.094 ± 0.055
	I309A	NA	15 ± 1.2	0.005 ± 0.0009
	R306K	NA	6.2 ± 0.88	40 ± 15
	Q105A	NA	4.5 ± 0.49	16 ± 4.8
	W279F	NA	0.88 ± 13	0.64 ± 0.12
	W279M	NA	0.43 ± 0.053	0.45 ± 0.085
	I309A/W279F	NA	4.5 ± 1.2	0.20 ± 0.010
	I309A/W279M	NA	2.4 ± 1.2	0.44 ± 0.058
 2a	NA	WT	2.4 ± 0.11	3.8 ± 0.15
	NA	V279L	6.9 ± 1.3	18.2 ± 3.2
	NA	V279I	7.3 ± 1.2	9.7 ± 0.81
	NA	V279A	10 ± 1.1	5.7 ± 1.8
	NA	R294K	5.9 ± 1.6	4.4 ± 1.5
	NA	Q102A	11 ± 1.4	3.9 ± 1.4
	NA	W267F	14 ± 1.9	7.7 ± 1.2
	NA	W267M	14 ± 1.6	38 ± 6.7

^a HEK293 cells were transfected for 48 h with 0.8 μg/mL of plasmid DNA encoding for TRH-R1, TRH-R2, or a mutant receptor and equilibrium binding constants were determined as described in Methods. Data are presented as the mean ± sem from three independent experiments performed in duplicates. NA = not applicable.

concentration of the radioligand (Figure 4C), which is consistent with competitive character of interaction of these ligands with TRH-R1.

To test the veracity of our docking model further, binding analyses of **2a** to a number of TRH-R1 and TRH-R2 mutants were performed (Table 1 and Supplementary Figure 3). According to the model, Arg306, a residue in TM-7 that is known to interact with Pro-NH₂ of TRH,²⁰ appears to form a hydrogen bond with the amide carbonyl of **2a** (Figure 5A,B). Substitution of Arg306 by Lys reduced affinity for **2a** by 200-fold, indicating its important role in **2a** binding. In contrast, substitution of the corresponding residue in TRH-R2 (Arg294Lys) shows no effect on **2a** binding, revealing an important difference in binding modes of **2a** to TRH-R1 and TRH-R2. According to the model of the TRH-R1/**2a** complex, Asp195 in TM-5 acts in conjunction with Arg306 to position **2a** within the binding pocket by formation of a H-bond with the amide hydrogen of **2a** (Figure 5A,B). However, substitutions of Asp195 abolish high affinity binding of MeTRH (not shown), thus preventing performance of competition binding experiments to evaluate **2a** affinity at this mutant TRH receptor.

Ile309 in TM-7 of TRH-R1 (Val297 in TRH-R2) sits at the bottom of the TRH binding cavity and represents the only difference in composition of the ligand binding pockets in the models of TRH-R1 and TRH-R2. Ile309 directly contacts one of the phenyl rings of **2a** (Figure 5B), raising the possibility that the Val/Ile variation may contribute to TRH-R1 isotype selectivity of **2a** through formation of additional hydrophobic contacts. Mutagenesis studies revealed that space-generating substitutions at this position in TRH-R1 increase affinity for **2a**. The potency of **2a** was as much as 1100-fold higher for alanine at position 309 as compared to leucine (Table 1). It is possible that extra space in the proximity of a phenyl ring of **2a** causes it to shift deeper into the transmembrane domain,

thereby optimizing existing interactions with key residues and/or allowing new interactions to form. According to the model of TRH-R1, Ile309 flanks Trp279 in TM-6, restricting its side chain to pointing outside of the ligand binding pocket (Figure 5A,B). Thus preventing its interaction with the bound ligand. Consistent with the model, substitution of Trp279 by smaller Phe or Met in TRH-R1 has no effect on **2a** binding (Table 1). However, in the Ile309Ala mutant receptor, substitution of Trp279 by Phe or Met results in 40- and 90-fold reduced affinities for **2a**, respectively (Table 1). This finding is consistent with the idea that reduced bulkiness in the vicinity of Trp279 in the Ile309Ala mutant allows its access to the ligand binding cavity and interaction with the bound **2a**, thereby contributing to the increased affinity of **2a** in this mutant compared to TRH-R1. In TRH-R2, by contrast, the nature of the residue at position 297 (corresponding to position 309 in TRH-R1) has no significant effect on **2a** binding (Table 1). These results support the model of the **2a**/TRH-R1 complex, but they do not support a role of the Ile/Val variation in **2a** isotype selectivity; they do further indicate that different interactions are involved in the formation of **2a** complexes with TRH-R1 and TRH-R2. The described relationships between the affinity of **2a** and the nature of the residue at position 309 in TRH-R1 may be valuable for future design of new ligands with improved potency and/or selectivity.

In the model of the TRH-R1/TRH complex, Gln105 (Gln102 in TRH-R2), located at the entrance of the ligand binding pocket, is situated in an outward pointed direction, therefore having no direct interaction with bound TRH (Figure 5A). In support of the model, the substitution of Gln105 by Ala does not affect TRH binding in TRH-R1 and TRH-R2 (Table 1). Conformational analysis of the residues in TRH-R1 reveals a high degree of flexibility associated with Gln105, allowing it access to the ligand binding pocket (Figure 5B). By approaching the ligand

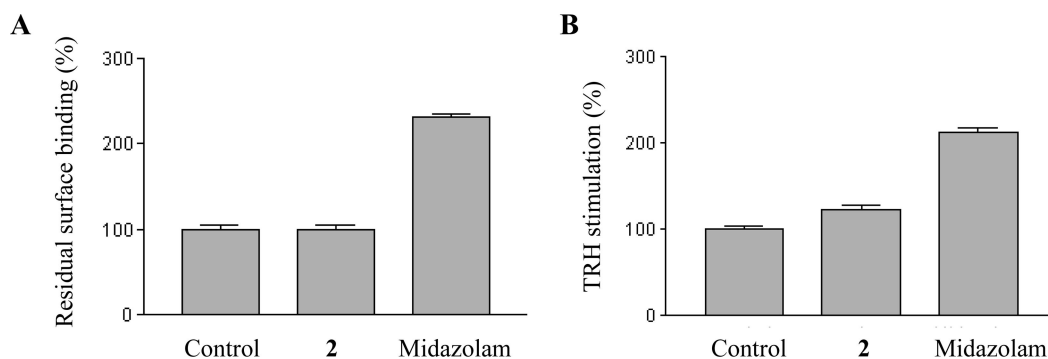


Figure 6. Effect of prolonged exposure to **2** or midazolam on the surface expression and signaling of TRH-R1. HEK293 cells stably expressing a low level of TRH-R1 (clone R1-17, ~70 000 receptors/cell) (see Engel, S.; Gershengorn, M. C. *J. Biol. Chem.* **2006**, *281*, 13103) were incubated without (control) or with 20 μ M of **2** or midazolam in DMEM (2% of heat-deactivated FBS) for 16 h at 37 $^{\circ}$ C. (A) After washing with HBSS (10% HEPES, pH 7.4), the cells were incubated for 1 min with ice-cold acid solution (0.2 M acetic acid, 0.5 M NaCl, pH 2.5) to remove the bound compounds, followed by wash (\times 3) with HBSS. The cells were incubated in the presence of 10 nM [3 H]MeTRH for 7 h at 4 $^{\circ}$ C, and specific binding was determined as described. (B) The cells were washed five times (10 min of incubation each) with HBSS at room temperature, and TRH-stimulated release of the intracellular Ca^{2+} was measured in the presence of 1 nM TRH (EC_{50} concentration) using FLIPR, as described in Methods. All data are presented as the mean \pm sem from three independent experiments performed in triplicate.

binding cavity, the Gln105 field of interaction with the H-donor/acceptor probe (Grid, see Methods) contributed to the selection of **2a** in the virtual screening by superimposition with one of its benzodioxin oxygens (not shown). A similar analysis in TRH-R2 revealed that Gln102 is conformationally restricted in the position outside of the binding pocket, making its interaction with the bound **2a** highly unlikely. In agreement with the model, the substitution of Gln105 in TRH-R1 by alanine reduced the binding affinity of **2a** by more than 50-fold (Table 1), whereas the corresponding substitution in TRH-R2 (Gln102Ala) showed no effect on **2a** binding. In fact, **2a** exhibits reversed selectivity for the Gln to Ala variants of TRH receptors, indicating that interaction of Gln105 with the bound ligand may contribute to **2a** TRH-R1 selectivity. Alternatively, the highly flexible Gln105 located at the entrance of the ligand binding cavity may facilitate **2a** transition into the TMD of TRH-R1 by formation of transient interactions with the ligand. Identification of Gln105 as a potential interaction site for **2a** exemplifies the need to use the entire available binding potential in formulation of a receptor-based pharmacophore, rather than the binding determinants of the cognate ligand only. Overall, the mutagenesis studies support the verity of the model of **2a**/TRH-R1 complex. Furthermore, they demonstrate that **2a** and TRH bind to TRH receptors by interacting with different transmembrane domain residues, and that different interactions are involved in stabilization of **2a** in TRH-R1 and TRH-R2, despite the similarities of their sites for interaction with TRH.

Finally, to begin to gauge the utility of this novel TRH receptor antagonist, we studied its effects on TRH receptors upon prolonged cellular exposure. Benzodiazepines (and their analogues) are the only class of nonpeptide compounds known to antagonize TRH signaling.⁴⁰ However, there are several disadvantages to their use as in vivo probes of inhibition of TRH signaling. For example, prolonged exposure of TRH receptor-expressing cells to benzodiazepines results in an increased number of surface receptors and potentiation of the TRH response (Figure 6 and ref 44), thereby compromising the antagonistic effect of these compounds. In contrast to benzodiazepines, prolonged incubation of TRH-R-expressing cells with **2** does not significantly affect surface expression of TRH

receptors or efficacy of TRH signaling (Figure 6). This feature of **2** represents a significant advantage over benzodiazepines for application in intact animals.

Conclusion

Virtual screening has been used in many efforts to identify novel small molecule ligands for diverse cellular targets including kinases, phosphatases, and transcription factors. Novel compounds originating from in silico methods have entered clinical evaluation in disease states such as cancer and diabetes. However, virtual methods targeting GPCRs have trailed behind, owing in large part to structural uncertainty of the receptors and a lack of novel in silico methods. The virtual screening methodology described in this study allows for a more inclusive representation of the structural potential available for interaction with artificial ligands, thereby increasing the likelihood of identification of ligands with diverse chemical scaffolds and potentially different binding modalities. By employing both an expanded interaction potential that differs from that utilized by the natural ligand and conformational flexibility within the binding cavity, and by minimizing the usage of scoring functions, chemically diverse antagonists of TRH receptors have been identified. Of note, these ligands are capable of distinguishing between TRH receptor isoforms that share nearly identical structural determinants for TRH binding and represent the first known small molecule ligands with a significant degree of TRH receptor isoform selectivity. Also, the chemical diversity of the new ligands and corresponding variation in their binding affinities can contribute to development of structure-activity

(44) Heinfink, M.; Nussenzweig, D. R.; Grimberg, H.; Lupu-Meir, M.; Oron, Y.; Gershengorn, M. C. *Mol. Endocrinol.* **1995**, *9*, 1455–1460.

- (45) Rasmussen, S. G.; Choi, H. J.; Rosenbaum, D. M.; Kobilka, T. S.; Thian, F. S.; Edwards, P. C.; Burghammer, M.; Ratnala, V. R.; Sanishvili, R.; Fischetti, R. F.; Schertler, G. F.; Weis, W. I.; Kobilka, B. K. *Nature* **2007**, *445*, 383–387.
- (46) Rosenbaum, D. M.; Cherezov, V.; Hanson, M. A.; Rasmussen, S. G.; Thian, F. S.; Kobilka, T. S.; Choi, H. J.; Yao, X. J.; Weis, W. I.; Stevens, R. C.; Kobilka, B. K. *Science* **2007**, *318*, 1266–1273.
- (47) Cherezov, V.; Rosenbaum, D. M.; Hanson, M. A.; Rasmussen, S. G.; Thian, F. S.; Kobilka, T. S.; Choi, H. J.; Kuhn, P.; Weis, W. I.; Kobilka, B. K.; Stevens, R. C. *Science* **2007**, *318*, 1258–1265.
- (48) Ferrara, P.; Gohlke, H.; Price, D. J.; Klebe, G.; Brooks, C. L., III *J. Med. Chem.* **2004**, *47*, 3032–3047.
- (49) Warren, G. L.; Andrews, C. W.; Capelli, A. M.; Clarke, B.; LaLonde, J.; Lambert, M. H.; Lindvall, M.; Nevins, N.; Semus, S. F.; Senger, S.; Tedesco, G.; Wall, I. D.; Woolven, J. M.; Peishoff, C. E.; Head, M. S. *J. Med. Chem.* **2006**, *49*, 5912–5931.

relationships for application in drug design using *ligand-based* approaches. Finally, the selectivity and cellular effects exhibited by **2a** suggest that it may be useful as a probe to distinguish the physiological roles of TRH-R1 and TRH-R2 in animal models.

Acknowledgment. We thank Dr. Bruce Raaka and Dr. Oksana Gavrilova for advice and help in preparation of this manuscript. We thank Ms. Allison Peck for critical reading of this manuscript. We thank Mr. John Lloyd for HRMS data. A.O.C. gratefully acknowledges Dr. David Stanton for his helpful suggestions and discussions regarding the virtual screening methodology. This research was supported by the Intramural Research Program of the National Institute of Diabetes and Digestive and Kidney Diseases, the Molecular Libraries Initia-

tive of the National Institutes of Health Roadmap for Medical Research, the Intramural Research Program of the National Human Genome Research Institute, and the National Institute of Drug Abuse (Contract Y1-DA6002-02), National Institutes of Health.

Supporting Information Available: Elaboration of virtual screening procedure, structures of alternate ligands discovered, chemical synthetic methods and characterization of products and intermediates, crystallographic analysis of **10d** and determination of absolute configuration of **2a–d**. This material is available free of charge via the Internet at <http://pubs.acs.org>.

JA077620L